Parkinsonism and Related Disorders 62 (2019) 134–140

Contents lists available at ScienceDirect

Parkinsonism and Related Disorders

journal homepage: www.elsevier.com/locate/parkreldis

Associations between neuroanatomical abnormality and motor symptoms in paroxysmal kinesigenic dyskinesia

Hong-Fu Li[a,b,1], Liqin Yang[c,d,1], Dazhi Yin[c,1], Wan-Jin Chen[e], Gong-Lu Liu[a], Wang Ni[a,b], Ning Wang[e], Wenwen Yu[c], Zhi-Ying Wu[a,**], Zheng Wang[c,*]

[a] Department of Neurology and Research Center of Neurology in Second Affiliated Hospital, and Key Laboratory of Medical Neurobiology of Zhejiang Province, Zhejiang University School of Medicine, Hangzhou, China
[b] Department of Neurology and Institute of Neurology, Huashan Hospital, Fudan University, China
[c] Institute of Neuroscience, State Key Laboratory of Neuroscience, CAS Center for Excellence in Brain Science and Intelligence Technology, Shanghai Institute for Biological Sciences, Chinese Academy of Sciences, China
[d] Department of Radiology, Huashan Hospital, Fudan University, China
[e] Department of Neurology and Institute of Neurology, First Affiliated Hospital, Fujian Medical University, China

ARTICLE INFO

Keywords:
Paroxysmal kinesigenic dyskinesia
PRRT2 mutations
Motor symptoms
Corticospinal tract
Gray matter volume

ABSTRACT

Introduction: The pathophysiologic mechanism of paroxysmal kinesigenic dyskinesia (PKD) is largely unclear. Basal ganglia-thalamo-cortical circuit involvement is thought to underlie PKD pathophysiology. However, microstructural alternations in the motor circuit of PKD require further elucidation.

Methods: Diffusion tensor imaging and high-resolution T1-weighted imaging were performed on 30 PKD patients (15 *PRRT2* carriers, 15 *PRRT2* non-carriers) and 15 matched healthy controls. Tract-based spatial statistics were conducted on diffusion indices to examine microstructural integrity of white matter. Voxel-based morphometry analysis was used to examine volumetric changes of gray matter. Multiple regression was employed to test the contribution of demography, disease duration, and *PRRT2* status to pathological changes in brain structure.

Results: Six (including two novel) *PRRT2* mutations were identified in PKD patients who exhibited significantly reduced mean diffusivity mainly along the left corticospinal tract, and reduced gray matter volume in pre-supplementary motor area (preSMA) and right opercular part of inferior frontal gyrus (IFGoperc), compared to healthy controls. Both gray matter volume reductions in preSMA and diffusion indices of abnormal white matter negatively correlated with disease duration. Genotype-phenotype analysis revealed that *PRRT2* mutation carriers had earlier onset age, longer attacks, and a larger proportion of bilateral symptoms than non-carriers.

Conclusions: We observed that *PRRT2* mutations were associated with disease severity, while neuroanatomical abnormality was associated with disease duration in patients with PKD. Aberrant microstructural changes in preSMA and IFG areas, independent of mutation status, point to dysregulated motor inhibition in patients and provide new insights into neurobiological mechanisms underlying motor symptoms of PKD.

1. Introduction

Paroxysmal kinesigenic dyskinesia (PKD) is a rare movement disorder in which sudden initiated motion induces paroxysmal attacks of involuntary movements [1]. It is inherited in an autosomal dominant pattern and caused by mutation within *PRRT2* [2]. Although the clinical features of PKD have been well described, its pathophysiologic mechanisms await further elucidation. Dysfunction of brain subcortical regions, including the basal ganglia nuclei and thalamus, has been reported in PKD patients [3–6]. In addition, abnormal intrinsic activity in motor, somatosensory, and frontal areas has also been reported [7–11]. These findings suggest that the ganglia-thalamo-cortical circuit underlies the pathophysiology of PKD. PKD can therefore be considered a circuit disorder, and disruption of these circuits may cause PKD.

* Corresponding author. Institute of Neuroscience, State Key Laboratory of Neuroscience, Shanghai Institute for Biological Sciences, Chinese Academy of Sciences, 320 Yueyang Road, Shanghai, 200031, China.
** Corresponding author. Department of Neurology and Research Center of Neurology in Second Affiliated Hospital, and Key Laboratory of Medical Neurobiology of Zhejiang Province, Zhejiang University School of Medicine, 88 Jiefang Road, Hangzhou, 310009, China.
E-mail addresses: zhiyingwu@zju.edu.cn (Z.-Y. Wu), zheng.wang@ion.ac.cn (Z. Wang).
[1] These authors contributed equally to this work.

https://doi.org/10.1016/j.parkreldis.2018.12.029
Received 12 August 2018; Received in revised form 17 December 2018; Accepted 31 December 2018

Conventional MRI brain scanning of PKD cases has mostly revealed unremarkable findings. Two recent studies reported microstructural abnormality of thalamus in PKD, represented by increased fractional anisotropy [12,13], volume reduction, and regional shape deformation [12]. However, few studies have analyzed *PRRT2* status and the relationship of structural alteration with disease duration and/or *PRRT2* mutations. Although Long et al. recently investigated the association of thalamocortical networks and basal ganglia/cortical networks with disease duration and *PRRT2* status in PKD patients, only a small group of *PRRT2* mutated patients (n = 8) was included [14].

Here, we aimed to address the relationships between genetic mutations, structural profile of gray and white matter alterations, and clinical symptoms of PKD in a combined sample of patients (with and without *PRRT2* mutations), thereby establishing a link among genotypes, intermediate phenotypes (structural imaging), and behavior phenotypes (clinical symptoms). Diffusion tensor imaging (DTI) and tract-based spatial statistics (TBSS) were employed to characterize white matter changes between groups [15]. T1-weighted imaging and voxel-based morphometry (VBM) were applied to detect volumetric alterations of cortical and subcortical gray matter [16]. To examine the diffusion and volumetric characteristics of abnormalities in *PRRT2* carriers and non-carriers, and their relationship with clinical or genetic information of PKD, volume-of-interest (VOI) and multiple regression analyses were performed.

2. Participants

A total of 45 subjects were recruited for this study. Thirty PKD patients were further classified into 2 subgroups after genetic testing: 15 *PRRT2* mutation carriers (PKD_m, 14 males, 20 ± 3.3 years) and 15 non-carriers (PKD_n, 13 males, 17.9 ± 3.8 years). All patients met the Bruno criteria for a diagnosis of PKD and were independently evaluated by at least two senior neurologists [1]. Two PKD_m cases (6 and 11) were familial PKD, while others were sporadic PKD. One PKD_m patient (13) suffered from infantile convulsions. No migraine or seizure was reported in other cases. No notable abnormalities in standard MRI examination were observed in any subject and there was no occurrence of neurological/psychiatric disease or substance abuse in the control subjects. Demographic and clinical characteristics including age at onset, frequency and duration of attacks, and laterality were recorded for analysis. PKD patients were either drug-naive or had discontinued medication prior to study participation, with the exception of one patient who was taking carbamazepine. Most subjects (24/30) experienced an attack before MRI scanning (i.e., ictal stage; see Supplementary Table 1 for details). Healthy controls (HCs) were 15 age- and gender-matched subjects (12 males; age 19.1 ± 4.5). Age ($p = 0.92$, $t = -0.11$) and gender ($p = 0.16$, Pearson Chi-Square = 2.0) were matched between all PKD patients and HCs. All participants were right-handed Han Chinese. Protocols were approved by the ethics committees of Huashan Hospital, Fudan University; Second affiliated Hospital, Zhejiang University School of Medicine; and Shanghai Institutes for Biological Sciences, Chinese Academy of Sciences, respectively. Written informed consent was obtained from each subject or their legal guardian once a complete description of the protocols was provided.

3. Genetic investigation

Genomic DNA was extracted from peripheral blood using standard protocol (Qiagen, Hilden, Germany). Sanger sequencing was performed to search for variants in *PRRT2*, *MR-1*, and *SLC2A1*, as described in previous studies [2,17]. Briefly, forward and reverse primers were designed and PCR was carried out to amplify the entire exons and the intron-exon boundaries. After purification, direct sequencing was performed using the ABI 3730 Automated DNA Sequencer (Applied Biosystems, Foster City, CA, USA). SIFT, MutationTaster, and PolyPhen-2 were used to predict the pathogenicity of the identified variants.

4. MRI data acquisition

MRI data were acquired with a 12-channel head coil on a Siemens Tim Trio 3.0T scanner (Siemens Healthcare, Erlangen, Germany) at the Brain Imaging Center of the Institute of Neuroscience, Chinese Academy of Sciences, Shanghai. Each participant was instructed to lie supine in the scanner wearing ear plugs to muffle scanner noise, with their head snugly fixed by tight but comfortable foam pads. High-resolution T1-weighted images were acquired using a 3D magnetization prepared rapid gradient echo sequence (repetition time/echo time = 2300/3 ms, inversion time = 1000 ms, flip angle = 9°, field of view = 256 × 256 mm^2, voxel size = 1 × 1 × 1 mm^3, 176 consecutive sagittal slices, acceleration factor = 2). DTI data were acquired using a single-shot spin-echo EPI-based sequence with the following parameters: 67 axial slices, field of view = 220 × 220 mm^2, repetition time/echo time = 8000/83 ms, flip angle = 90°, with a 110 × 110 reconstruction matrix, yielding a 2 × 2 × 2 mm^3 voxel size, phase partial Fourier = 6/8, nine non-diffusion weighted (i.e., b = 0 s/mm^2) b0 images were added interleaved in 64 diffusion weight images (b = 700 s/mm^2). Data of one PKD_m subject and one PKD_n subject were excluded following imaging analysis due to poor image quality.

5. TBSS analysis

DTI data were first preprocessed using toolboxes within the FMRIB Software Library (FSL v5.0, http://www.fmrib.ox.ac.uk/fsl), including eddy current correction, brain extraction (using BET), and diffusion tensor fitting (using FDT). The diffusion tensor for each brain voxel was thus estimated and diagonalized to obtain three eigenvalues (λ1, λ2, and λ3). Voxel-wise values of diffusion-related indices were derived according to the following equations:

$$FA = \frac{\sqrt{(\lambda_1 - \lambda_2)^2 + (\lambda_2 - \lambda_3)^2 + (\lambda_3 - \lambda_1)^2}}{\sqrt{2}\sqrt{\lambda_1^2 + \lambda_2^2 + \lambda_3^2}}$$

$$MD = \frac{\lambda_1 + \lambda_2 + \lambda_3}{3}$$

$$AD = \lambda_1,$$

$$RD = \frac{\lambda_2 + \lambda_3}{2}$$

where FA is fractional anisotropy, MD is mean diffusivity, AD is axial diffusivity, and RD is radial diffusivity.

After preprocessing, whole brain analysis of the two most frequently used diffusion indices (i.e., FA and MD) was performed using TBSS in FSL following previously demonstrated techniques [15,18]. First, individual FA images were aligned and normalized to the Montreal Neurological Institute standard space via the FMRIB58_FA template. A mean FA image was then created and thresholded (FA > 0.2) to form a skeleton mask, after which individual FA images were projected onto this common skeleton. Standard-space MD, AD, and RD images were also produced by applying the above warping and projection of FA to corresponding individual images.

Voxel-wise statistical analysis of differences in FA and MD between PKD patients (PKD_m and PKD_n) and HCs were performed using a non-parametric permutation method ("randomize" program) with 5000 permutations. Threshold-free cluster enhancement (TFCE) was used to find significant differences at $p < 0.05$, after family-wise error correction for multiple comparisons. Regions with significant differences were identified according to the Johns Hopkins University (JHU) —ICBM-DTI-81 white matter labels atlas and JHU-WM Tractography Atlas in FSL.

6. Voxel-based morphometry (VBM) analysis

We performed VBM analysis on T1-weighted images using the SPM8 software package (http://www.fil.ion.ucl.ac.uk/spm/). T1-weighted images of each participant were segmented into gray matter, white matter, and cerebrospinal fluid. Each participant's gray matter and white matter images were nonlinearly registered with the DARTEL method and transformed to the MNI standard space. The warped gray matter images were then modulated by Jacobian determinants, so that volume information was included in these modulated images. Finally, the resultant maps were smoothed with a 6-mm full width at half maximum Gaussian kernel.

PKD patients (both PKD_m and PKD_n) and HCs were compared using two-tailed independent samples t-tests. The threshold for statistical significance was set at $p < 0.05$ with AlphaSim correction for multiple comparisons (i.e. a combined cutoff value of $p < 0.0005$ and a minimum cluster size of 60 voxels).

7. VOI analysis of white matter and gray matter abnormalities

To quantitatively investigate the white matter diffusion characteristics and gray matter volumetric differences among the three groups (PKD_m, PKD_n, and HCs), VOI analyses were performed on regions showing significant abnormalities between all PKD patients and HCs. This procedure initially required extracting binary white matter or gray matter VOI masks based on clusters showing significant FA/MD or gray matter volume differences in TBSS or VBM analysis, respectively. The mean value of diffusion indices or gray matter volume of each VOI was then calculated for each subject. Finally, we conducted statistical comparisons among PKD_m, PKD_n, and HCs using two-tailed two sample t tests. A Bonferroni corrected threshold of $p < 0.05$ (i.e., $p < 0.05/3 = 0.017$ for three comparisons) was considered to be statistically significant.

8. Multiple regression analysis

To determine the quantitative contribution of various factors to pathological changes in the white matter diffusion indices or gray matter volume of PKD patients in each identified region, we performed the following multiple regression:

$$\text{Diffusion indices / gray matter volume} = \beta_0 + \beta_1 \times A + \beta_2 \times D + \beta_3 \times M$$

where A is a vector for age, D stands for a vector for disease duration, and M reflects *PRRT2* mutation status (1 = with mutations, 0 = without mutations). The β_i ($i = 0, 1, 2, 3$) values are corresponding coefficients. We evaluated R squared and p value (F test) for the linear regression model, as well as the contribution of each factor to the diffusion indices or gray matter volume using t-tests, with $p < 0.05$ considered statistically significant. For factors with larger effects on gray matter volume or diffusion indices, we conducted further Pearson correlation analysis.

9. Results

9.1. PRRT2 mutations identified in PKD cases

We identified a total of six different *PRRT2* mutations in 15 of 30 cases. Among the mutation carriers, 8 cases (53.33%) harbored c.649dupC mutation, 2 cases carried c.649delC (p.R217Efs*12) mutation, 2 cases carried a c.931C > T (p.R311W) mutation, and one case carried c.133-136delCCAG mutation. In addition, we detected 2 novel *PRRT2* mutations (Supplementary Fig. 1), c.856G > A (p.V286M) in one case, and c.640delG (p.A214Pfs*15) in another one case. The frequency of c.856G > A was 0.000008628 in ExAC database. It was predicted to be deleterious by SIFT, MutationTaster, and PolyPhen-2. The frameshift mutation c.640delG was absent in ExAC database and was presumed to be pathogenic. No variant of *MR-1* or *SLC2A1* was identified in the 15 PKD_n cases.

9.2. Association between clinical features and PRRT2 mutations

Detailed demographics, clinical and genetic characteristics of PKD cases are summarized in Supplementary Table 1. Overall, the male-to-female ratio of patients was 9:1 (27 males, 3 females), and did not significantly differ between the *PRRT2* mutation carriers and non-carriers. The mean age at onset for PKD_m was significantly lower than for PKD_n ($p = 0.005$). *PRRT2* mutations carriers had a longer duration of attacks than non-carriers ($p = 0.014$). The frequency of attacks was not significantly different ($p = 0.093$). Attacks were bilateral in 100% PKD_m cases and 40% (6/15) of PKD_n cases ($p = 0.0007$). In addition, 80% (12/15) of PKD_m cases presented with the choreoathetosis phenotype, while 73% (11/15) of PKD_n cases exhibited the dystonia phenotype ($p = 0.0034$).

9.3. Abnormalities of white matter and gray matter

Compared to healthy subjects, PKD patients exhibited significantly reduced mean diffusivity (MD, $p < 0.05$, TFCE-corrected) in the left hemisphere, mainly along the left corticospinal tract, involving the white matter in conjunction with left precentral gyrus (M1), postcentral gyrus (S1) and supplementary motor area (SMA), part of left superior corona radiata, and left posterior limb of internal capsule. The MD of a section of the left anterior thalamic radiation passing through the anterior limb of the internal capsule was also reduced (Fig. 1A). FA did not differ significantly in patients. We also found significantly reduced gray matter volume (modulated density) ($p < 0.05$, AlphaSim corrected) in the presupplementary motor area (preSMA, Montreal Neurological Institute coordinates: [5, 29, 50], 95 voxels) and the opercular part of inferior frontal gyrus (IFGoperc, Montreal Neurological Institute coordinates: [51, 20, 36], 60 voxels) in PKD patients compared to HCs (Fig. 1B).

In white matter regions with significant group differences (Fig. 1A), reductions of MD, AD and RD in both PKD_m (mean values: $MD = 6.8 \times 10^{-4}\,mm^2/s$, $AD = 11.7 \times 10^{-4}\,mm^2/s$, $RD = 4.3 \times 10^{-4}\,mm^2/s$) and PKD_n (mean values: $MD = 6.9 \times 10^{-4}\,mm^2/s$, $AD = 11.8 \times 10^{-4}\,mm^2/s$, $RD = 4.4 \times 10^{-4}\,mm^2/s$) groups were observed compared to healthy subjects (mean values: $MD = 7.5 \times 10^{-4}\,mm^2/s$, $AD = 12.6 \times 10^{-4}\,mm^2/s$, and $RD = 4.9 \times 10^{-4}\,mm^2/s$) (Fig. 2A). However, no significant difference was found between *PRRT2* carriers and *PRRT2* non-carriers, although the group mean values of PKD_m were slightly lower than those of PKD_n. In gray matter regions with significant group differences (Fig. 1B), significant decreases in gray matter volume (modulated density) in both PKD_m (mean values: 0.59 for preSMA and 0.26 for IFGoperc) and PKD_n (mean values: 0.59 for preSMA and 0.27 for IFGoperc) were observed relative to HCs (mean values: 0.68 for preSMA and 0.33 for IFGoperc) (Fig. 2B). We found no significant differences of VOI-based gray matter volume between PKD_m and PKD_n.

9.4. Associations between PRRT2 mutation, structural abnormalities and symptoms

The proposed linear regression models were well fitted for diffusion indices including MD ($p = 0.02$, $R^2 = 0.33$) and AD ($p = 0.008$, $R^2 = 0.39$), but marginal for RD ($p = 0.07$, $R^2 = 0.25$). Moreover, only disease duration significantly affected the MD ($p = 0.008$), AD ($p = 0.002$), and RD ($p = 0.036$), while age ($p > 0.1$) and status of *PRRT2* mutations ($p > 0.1$) did not (Table 1). In addition, we observed that MD ($r = -0.54$, $p = 0.003$) (Fig. 3A), AD ($r = -0.58$, $p = 0.001$) (Fig. 3B), and RD ($r = -0.47$, $p = 0.011$) (Fig. 3C) were negatively

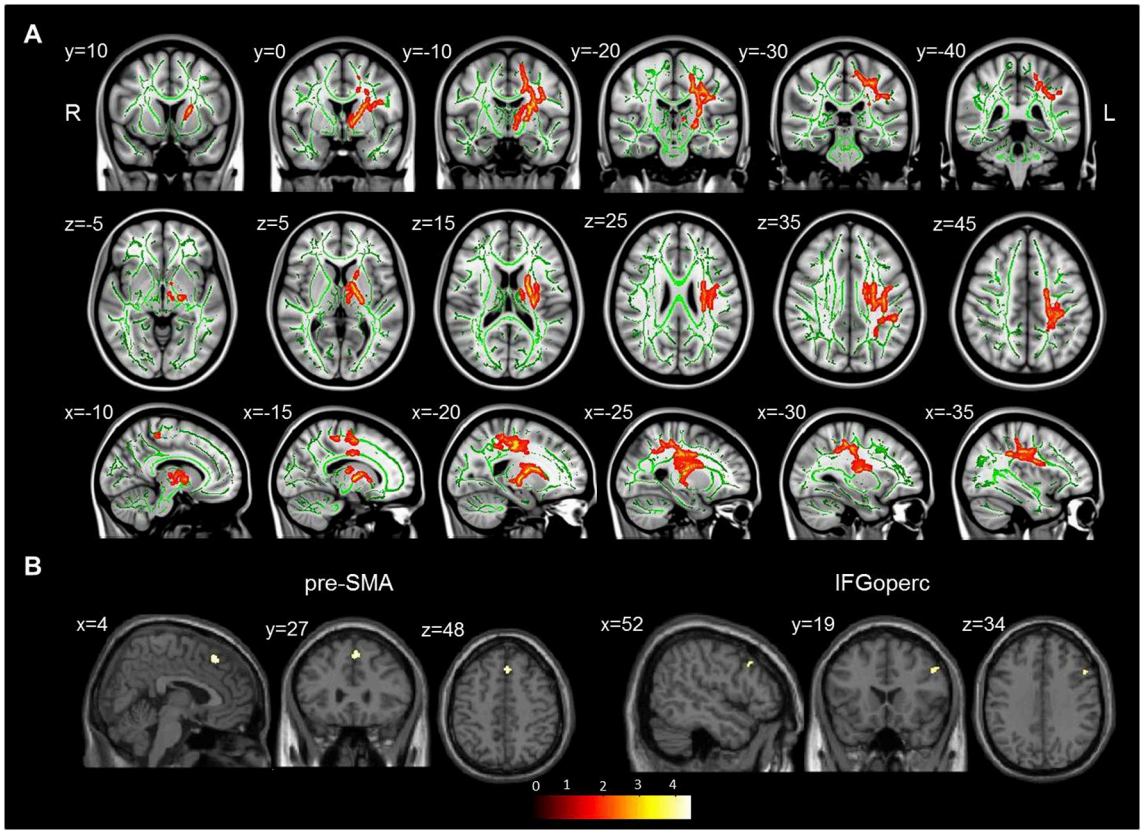

Fig. 1. (A) TBSS analysis results of mean diffusivity (MD) maps. Areas in Yellow-Red are regions where MD was significantly reduced ($p < 0.05$, corrected by TFCE and FWE for multiple comparisons) in PKD patients relative to healthy controls. For better visualization, regions showing reduced MD are thickened using TBSS_fill script implemented in FSL software. Results are overlaid on the MNI152-T1 template and the mean FA skeleton (green). (B) VBM analysis shows significantly reduced gray matter volume in PKD patients compared with healthy controls. The statistical threshold was set at $p < 0.05$ using the AlphaSim correction for multiple comparisons with a combined cutoff value of $p < 0.0005$ and a minimum cluster size of 60 voxels. x, y, and z denote MNI coordinates. TBSS = tract-based spatial statistics, TFCE = threshold-free cluster enhancement, PKD = paroxysmal kinesigenic dyskinesia, MNI = Montreal Neurological Institute, L = left, and R = right. Colorbar indicates the t value. VBM = voxel-based morphometry, GM = gray matter, preSMA = pre-supplementary motor area, IFGoperc = opercular part of inferior frontal gyrus. (For interpretation of the references to colour in this figure legend, the reader is referred to the Web version of this article.)

correlated with disease duration.

The proposed linear regression models were well fitted for gray matter volume in the preSMA ($p = 0.04$, $R^2 = 0.29$), but not the IFGoperc ($p = 0.43$, $R^2 = 0.11$). Moreover, gray matter volume in the preSMA was solely affected by disease duration ($p = 0.014$), but not age ($p > 0.1$) or *PRRT2* mutation status ($p > 0.1$) (Table 1). We next determined that gray matter volume reduction in the preSMA ($r = -0.47$, $p = 0.012$) was negatively correlated with disease duration (Fig. 3D).

10. Discussion

Recent genetic studies have advanced our understanding of the molecular mechanisms of PKD, but a substantial gap in the correspondence between PKD-specific neuroplastic changes in brain networks and observed motor symptoms remains to be filled. Here, we used a multimodal imaging approach to demonstrate that both white matter fiber integrity along the left corticospinal tract and anterior thalamic radiation and gray matter volume in preSMA and right IFGoperc is significantly decreased in PKD patients. Interestingly, none of these imaging measures were related to the age or *PRRT2* mutation status of patients, although the reduction of white matter diffusivity and gray matter volumetric change in the preSMA correlated with disease duration. These findings suggest that microstructural alternations are associated with the clinical phenotypes of PKD rather than the *PRRT2* mutation status. In addition, aberrant changes in preSMA and IFG areas point to dysregulated motor inhibition in PKD patients. Our results provide new insights into the neurobiological mechanisms underlying the motor symptoms of PKD.

The corticospinal tract is of paramount importance within the motor system, particularly in the coordination of voluntary movement. Corticospinal tract axons originate in somatosensory and motor regions, travelling through the corona radiate, internal capsule, cerebral peduncles and brainstem, with the majority of fibers reaching the contralateral spinal cord [19,20]. Pathological changes in the anterior thalamic radiation indicate a disturbance of the thalamo-frontal connection in PKD. Considering that thalamocortical circuits are closely associated with the extrapyramidal loop, structural alterations in these fiber pathways may mediate PKD-related hyperactivity in thalamic, cortical and basal ganglia regions that has previously been reported [5,13,14]. Both the corticospinal tract and anterior thalamic radiation exhibited significant decreases in average molecular motion independent of tissue directionality (indexed by MD) in PKD patients compared to HCs. Examination of individual diffusion indices showed reductions in both AD and RD. RD specifically reflects diffusivity perpendicular to axonal fibers and is sensitive to pathological changes in myelin. In animal models, increased RD has been shown to accompany demyelinating degeneration [21]. Meanwhile, AD characterizes water diffusivity in the direction of the fiber tract, thereby providing an overall assessment of axonal integrity. Degenerative processes such as structural loss typically lead to increases in diffusivity (MD, RD, and AD), as have been reported in patients with epilepsy [22]. Conversely, decreases in these indices as observed here more likely suggest a different mechanistic process that may be involved in myelination, axonal

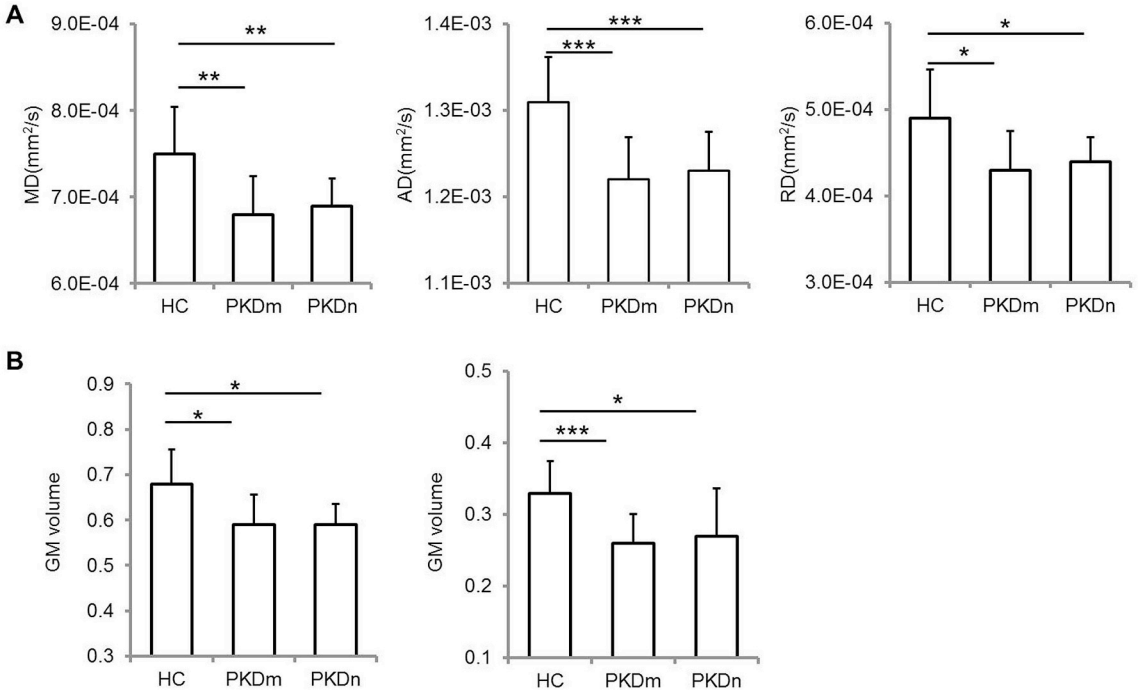

Fig. 2. (A) Quantitative comparisons of diffusion indices (i.e., MD, AD, and RD) within the white matter VOI from TBSS analysis results among PKD_m, PKD_n, and HCs. (B) Quantitative comparisons of GM volume (modulated density) within the pre-SMA (Left) and IFGoperc (Right) from VBM analysis results among PKD_m, PKD_n, and HCs. $*p < 0.01$, $**p < 0.001$, $***p < 0.0001$. A threshold of Bonferroni corrected $p < 0.05$ (i.e., $p < 0.05/3 = 0.017$ for three times of comparisons) was considered to be statistically significant. MD = mean diffusivity, AD = axial diffusivity, RD = radial diffusivity, PKD_m = paroxysmal kinesigenic dyskinesia with PRRT2 mutations, PKD_n = paroxysmal kinesigenic dyskinesia without PRRT2 mutations, HCs = healthy controls, TBSS = tract-based spatial statistics. VBM = voxel-based morphometry, GM = gray matter, preSMA = pre-supplementary motor area, IFGoperc = opercular part of inferior frontal gyrus.

narrowing or changes in cell permeability [23,24], rather than degenerative processes. It has been shown that *PRRT2* localizes mostly in axons of glutamatergic synapses [25]. PRRT2 silencing in primary neurons decreases synaptic density and alters nerve terminal ultrastructure [26]. Defects in axons may therefore occur in neurons where PRRT2 is highly expressed. The inverse relationship between disease duration and all three diffusion indices indicates an accumulated effect of PKD-specific aberrant changes in white matter architecture over time. Note that we observed a biased lateralization of white matter alterations here, which implies preferential impairment of the dominant hemisphere of patients as all subjects were right-handed.

Despite the overlap in symptomology between other forms of dyskinesia and PKD, a key discerning feature of PKD is kinesigenic symptom elicitation. The cortical areas found to exhibit PKD-related changes in this study, the right IFG and preSMA, are centrally involved in motor inhibition, i.e. discontinuing an already initiated response [27,28]. Efficient response inhibition could be achieved by an indirect pathway through the IFG/preSMA connection with the striatum, or by a hyperdirect pathway through their connection with the subthalamic nucleus [29,30]. Thus, the detected impairments in these two regions are likely related to deficits in motor switching and inhibition in PKD patients. While right IFG (specifically, the pars opercularis as detected in this study) has been recently conceptualized as a 'brake' in response inhibition which could outright stop or partially pause actions emerging externally or internally [31], activity in the preSMA was found to precede activity in right IFG [28,32] and may play a role in conflict detection and response, and switching and updating in motor procedures [29,32,33]. The significant correlations between gray matter volume in preSMA and disease duration could signify microstructural atrophy of preSMA throughout years of illness with repeated brief attacks but inefficient motor switching and inhibition, which may constitute a potential target for the future development of therapeutic treatments.

Overall, the phenotypes of our PKD cohort were relatively

Table 1
Statistics of multiple regression for diffusivity indices and GM volume.

	R2	F-test		T-test								
		p	F	Age			Duration			Gene Status		
				beta	p	t	beta	p	t	beta	p	t
Diffusivity indices												
MD	0.33	0.02	3.91	7.5×10^{-7}	0.74	0.34	-5.9×10^{-6}	0.008	−2.87	1.5×10^{-5}	0.30	1.06
AD	0.39	0.008	5.02	1.9×10^{-6}	0.46	0.74	-8.1×10^{-6}	0.002	−3.44	2.1×10^{-5}	0.22	1.27
RD	0.25	0.07	2.61	1.7×10^{-7}	0.94	0.07	-4.8×10^{-6}	0.036	−2.23	1.2×10^{-5}	0.42	0.82
GM volume												
preSMA	0.29	0.04	3.22	0.001	0.75	0.32	−0.008	0.014	−2.65	0.033	0.15	1.51
IFGoperc	0.11	0.43	0.96	0.002	0.60	0.54	−0.005	0.12	−1.59	0.013	0.57	0.58

Note: MD = mean diffusivity, AD = axial diffusivity, RD = radial diffusivity, GM = gray matter, preSMA = pre-supplementary motor area, IFGoperc = opercular part of inferior frontal gyrus.

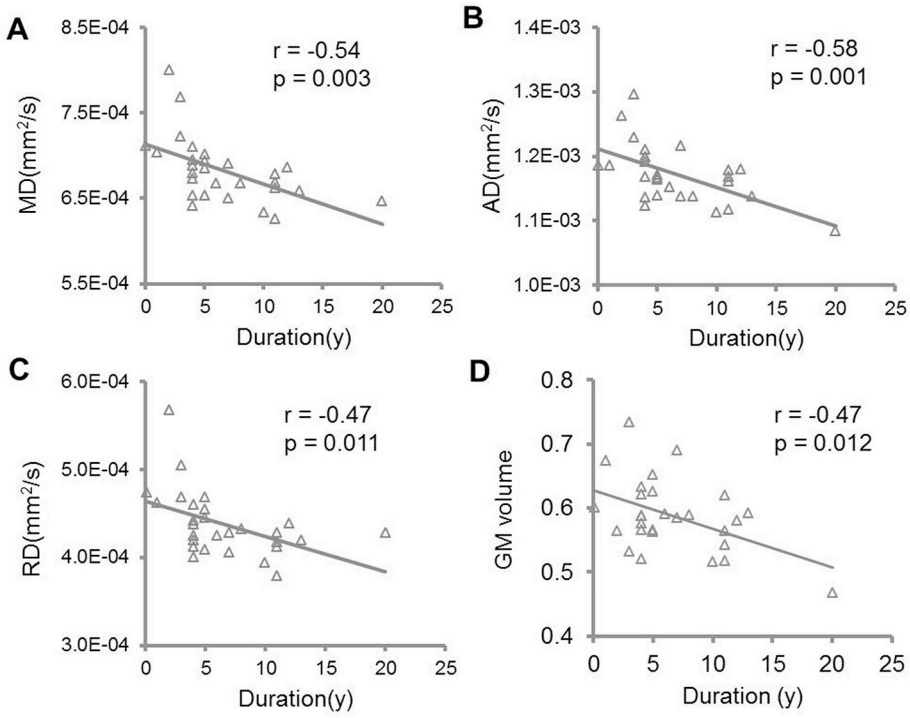

Fig. 3. (A, B, C) Significant correlations between diffusion indices (i.e., MD, AD, and RD) within the white matter VOI from TBSS result and disease duration of PKD patients. (D) Significant correlation between GM volume (modulated density) in the pre-SMA from VBM analysis result and disease duration of PKD patients. MD = mean diffusivity, AD = axial diffusivity, RD = radial diffusivity, preSMA = pre-supplementary motor area, GM = gray matter, and y = years.

homogeneous. Only one case suffered from infantile convulsions. No other concomitant symptoms (such as migraine, seizure, or ataxia) were reported in the remaining cases. In addition to the *PRRT2* gene, all patients underwent sequencing of *MR-1* and *SLC2A1* genes to exclude paroxysmal non-kinesigenic dyskinesia (PNKD) and paroxysmal exercise-induced dyskinesia (PED). More importantly, the majority of our PKD cases were in a drug-naive or withdrawal period before MRI scanning. This is different to one other comparable study and may explain the discrepancy between our findings and theirs [6]. A limitation of our study is that we did not screen all the genes (only 3 major genes) associated with paroxysmal dyskinesias. In addition, our patient sample was still relatively small; current results should be interpreted with caution. Future longitudinal research with a larger dataset is needed to examine structural or functional responses in the pathological circuits induced by medication treatment in PKD.

Authors' roles

Dr. Li: data acquisition, statistical analysis and interpretation, and drafting the manuscript. Dr. Yang: data acquisition, analysis and interpretation, and drafting the manuscript. Dr. Chen: data acquisition and analysis. Dr. Yin: data analysis and interpretation, and drafting the manuscript. Dr. Liu: data acquisition and analysis. Dr. Ni: data acquisition and analysis. Dr. Wang: data acquisition and analysis. Ms. Yu: data acquisition and analysis. Dr Wu: study design and conceptualization, data acquisition, analysis and interpretation, critical revision of the manuscript. Prof. Wang: funding, study design and conceptualization, data acquisition, analysis and interpretation, critical revision of the manuscript. All authors contributed to the writing of this manuscript.

Financial disclosures/conflict of interest

All the authors reported no disclosures.

Funding

Funding for this study was granted by the Hundred Talent Program of the Chinese Academy of Sciences (Technology) and the Strategic Priority Research Program (B) of the Chinese Academy of Sciences (XDB02050006) and the National Natural Science Foundation of China (81571300, 81527901, 81330025, 81500973, and 31600869), and Scientific Research project of Huashan Hospital, Fudan University (2016QD085).

Acknowledgments

We sincerely acknowledge the participants for their willingness to take part in this study. We also thank Kristina Zeljic (Chinese Academy of Sciences) to copyedit our manuscript.

Appendix A. Supplementary data

Supplementary data to this article can be found online at https://doi.org/10.1016/j.parkreldis.2018.12.029.

References

[1] M.K. Bruno, M. Hallett, K. Gwinn-Hardy, B. Sorensen, E. Considine, S. Tucker, D.R. Lynch, K.D. Mathews, K.J. Swoboda, J. Harris, B.W. Soong, T. Ashizawa, J. Jankovic, D. Renner, Y.H. Fu, L.J. Ptacek, Clinical evaluation of idiopathic paroxysmal kinesigenic dyskinesia: new diagnostic criteria, Neurology 63 (2004) 2280–2287.

[2] W.J. Chen, Y. Lin, Z.Q. Xiong, W. Wei, W. Ni, G.H. Tan, S.L. Guo, J. He, Y.F. Chen, Q.J. Zhang, H.F. Li, Y. Lin, S.X. Murong, J. Xu, N. Wang, Z.Y. Wu, Exome sequencing identifies truncating mutations in PRRT2 that cause paroxysmal kinesigenic dyskinesia, Nat. Genet. 43 (2011) 1252–1255.

[3] E.Y. Joo, S.B. Hong, W.S. Tae, J.H. Kim, S.J. Han, D.W. Seo, K.H. Lee, M.H. Kim, S. Kim, M.H. Lee, B.T. Kim, Perfusion abnormality of the caudate nucleus in patients with paroxysmal kinesigenic choreoathetosis, Eur. J. Nucl. Med. Mol. Imaging 32 (2005) 1205–1209.

[4] S. Shirane, M. Sasaki, D. Kogure, H. Matsuda, T. Hashimoto, Increased ictal perfusion of the thalamus in paroxysmal kinesigenic dyskinesia, J. Neurol. Neurosurg. Psychiatry 71 (2001) 408–410.

[5] B. Zhou, Q. Chen, Q. Zhang, L. Chen, Q. Gong, H. Shang, H. Tang, D. Zhou, Hyperactive putamen in patients with paroxysmal kinesigenic choreoathetosis: a resting-state functional magnetic resonance imaging study, Mov. Disord. 25 (2010) 1226–1231.

[6] M.O. Kim, J.H. Im, C.G. Choi, M.C. Lee, Proton MR spectroscopic findings in paroxysmal kinesigenic dyskinesia, Mov. Disord. 13 (1998) 570–575.

[7] W.Y. Hsu, S.Y. Kwan, K.K. Liao, R.S. Chen, Y.Y. Lin, Altered inhibitory modulation

of somatosensory cortices in paroxysmal kinesigenic dyskinesia, Mov. Disord. 28 (2013) 1728–1731.
[8] P. Mir, Y.Z. Huang, F. Gilio, M.J. Edwards, A. Berardelli, J.C. Rothwell, K.P. Bhatia, Abnormal cortical and spinal inhibition in paroxysmal kinesigenic dyskinesia, Brain 128 (2005) 291–299.
[9] C. Luo, Y. Chen, W. Song, Q. Chen, Q. Gong, H.F. Shang, Altered intrinsic brain activity in patients with paroxysmal kinesigenic dyskinesia by PRRT2 mutation: altered brain activity by PRRT2 mutation, Neurol. Sci. 34 (2013) 1925–1931.
[10] J. Ren, D. Lei, T. Yang, D. An, F. Xiao, L. Li, X. Huang, Q. Gong, D. Zhou, Increased interhemispheric resting-state functional connectivity in paroxysmal kinesigenic dyskinesia: a resting-state fMRI study, J. Neurol. Sci. 351 (2015) 93–98.
[11] Z.R. Liu, H.H. Miao, Y. Yu, M.P. Ding, W. Liao, Frequency-specific local synchronization changes in paroxysmal kinesigenic dyskinesia, Medicine 95 (2016) e3293.
[12] J.H. Kim, D.W. Kim, J.B. Kim, S.I. Suh, S.B. Koh, Thalamic involvement in paroxysmal kinesigenic dyskinesia: a combined structural and diffusion tensor MRI analysis, Hum. Brain Mapp. 36 (2015) 1429–1441.
[13] B. Zhou, Q. Chen, Q. Gong, H. Tang, D. Zhou, The thalamic ultrastructural abnormalities in paroxysmal kinesigenic choreoathetosis: a diffusion tensor imaging study, J. Neurol. 257 (2010) 405–409.
[14] Z. Long, Q. Xu, H.H. Miao, Y. Yu, M.P. Ding, H. Chen, Z.R. Liu, W. Liao, Thalamocortical dysconnectivity in paroxysmal kinesigenic dyskinesia: combining functional magnetic resonance imaging and diffusion tensor imaging, Mov. Disord. 32 (2017) 592–600.
[15] S.M. Smith, M. Jenkinson, H. Johansen-Berg, D. Rueckert, T.E. Nichols, C.E. Mackay, K.E. Watkins, O. Ciccarelli, M.Z. Cader, P.M. Matthews, T.E. Behrens, Tract-based spatial statistics: voxelwise analysis of multi-subject diffusion data, Neuroimage 31 (2006) 1487–1505.
[16] C.J. Honey, O. Sporns, L. Cammoun, X. Gigandet, J.P. Thiran, R. Meuli, P. Hagmann, Predicting human resting-state functional connectivity from structural connectivity, Proc. Natl. Acad. Sci. U. S. A 106 (2009) 2035–2040.
[17] H.F. Li, W.J. Chen, W. Ni, K.Y. Wang, G.L. Liu, N. Wang, Z.Q. Xiong, J. Xu, Z.Y. Wu, PRRT2 mutation correlated with phenotype of paroxysmal kinesigenic dyskinesia and drug response, Neurology 80 (2013) 1534–1535.
[18] D. Yin, X. Yan, M. Fan, Y. Hu, W. Men, L. Sun, F. Song, Secondary degeneration detected by combining voxel-based morphometry and tract-based spatial statistics in subcortical strokes with different outcomes in hand function, AJNR. Am. J. Neuroradiol. 34 (2013) 1341–1347.
[19] J.P. Seo, S.H. Jang, Different characteristics of the corticospinal tract according to the cerebral origin: DTI study, AJNR. Am. J. Neuroradiol. 34 (2013) 1359–1363.
[20] A. Kumar, C. Juhasz, E. Asano, S.K. Sundaram, M.I. Makki, D.C. Chugani, H.T. Chugani, Diffusion tensor imaging study of the cortical origin and course of the corticospinal tract in healthy children, AJNR. Am. J. Neuroradiol. 30 (2009) 1963–1970.
[21] S.K. Song, S.W. Sun, W.K. Ju, S.J. Lin, A.H. Cross, A.H. Neufeld, Diffusion tensor imaging detects and differentiates axon and myelin degeneration in mouse optic nerve after retinal ischemia, Neuroimage 20 (2003) 1714–1722.
[22] N.K. Focke, C. Diederich, G. Helms, M.A. Nitsche, H. Lerche, W. Paulus, Idiopathic-generalized epilepsy shows profound white matter diffusion-tensor imaging alterations, Hum. Brain Mapp. 35 (2014) 3332–3342.
[23] D. Qiu, L.H. Tan, K. Zhou, P.L. Khong, Diffusion tensor imaging of normal white matter maturation from late childhood to young adulthood: voxel-wise evaluation of mean diffusivity, fractional anisotropy, radial and axial diffusivities, and correlation with reading development, Neuroimage 41 (2008) 223–232.
[24] A. Imfeld, M.S. Oechslin, M. Meyer, T. Loenneker, L. Jancke, White matter plasticity in the corticospinal tract of musicians: a diffusion tensor imaging study, Neuroimage 46 (2009) 600–607.
[25] M. Li, F. Niu, X. Zhu, X. Wu, N. Shen, X. Peng, Y. Liu, PRRT2 mutant leads to dysfunction of glutamate signaling, Int. J. Mol. Sci. 16 (2015) 9134–9151.
[26] R. Erro, K.P. Bhatia, A.J. Espay, P. Striano, The epileptic and nonepileptic spectrum of paroxysmal dyskinesias: channelopathies, synaptopathies, and transportopathies, Mov. Disord. 32 (2017) 310–318.
[27] A.R. Aron, T.E. Behrens, S. Smith, M.J. Frank, R.A. Poldrack, Triangulating a cognitive control network using diffusion-weighted magnetic resonance imaging (MRI) and functional MRI, J. Neurosci. 27 (2007) 3743–3752.
[28] N.C. Swann, W. Cai, C.R. Conner, T.A. Pieters, M.P. Claffey, J.S. George, A.R. Aron, N. Tandon, Roles for the pre-supplementary motor area and the right inferior frontal gyrus in stopping action: electrophysiological responses and functional and structural connectivity, Neuroimage 59 (2012) 2860–2870.
[29] S. Jahfari, F. Verbruggen, M.J. Frank, L.J. Waldorp, L. Colzato, K.R. Ridderinkhof, B.U. Forstmann, How preparation changes the need for top-down control of the basal ganglia when inhibiting premature actions, J. Neurosci. 32 (2012) 10870–10878.
[30] S. Jahfari, L. Waldorp, W.P. van den Wildenberg, H.S. Scholte, K.R. Ridderinkhof, B.U. Forstmann, Effective connectivity reveals important roles for both the hyperdirect (fronto-subthalamic) and the indirect (fronto-striatal-pallidal) fronto-basal ganglia pathways during response inhibition, J. Neurosci. 31 (2011) 6891–6899.
[31] A.R. Aron, T.W. Robbins, R.A. Poldrack, Inhibition and the right inferior frontal cortex: one decade on, Trends Cognit. Sci. 18 (2014) 177–185.
[32] F.X. Neubert, R.B. Mars, E.R. Buch, E. Olivier, M.F. Rushworth, Cortical and subcortical interactions during action reprogramming and their related white matter pathways, Proc. Natl. Acad. Sci. U. S. A 107 (2010) 13240–13245.
[33] D.J. Sharp, V. Bonnelle, X. De Boissezon, C.F. Beckmann, S.G. James, M.C. Patel, M.A. Mehta, Distinct frontal systems for response inhibition, attentional capture, and error processing, Proc. Natl. Acad. Sci. U. S. A 107 (2010) 6106–6111.